PERGAMON

International Journal of Heat and Mass Transfer 43 (2000) 21–37

International Journal of HEAT and MASS TRANSFER

www.elsevier.com/locate/ijhmt

The importance of turbulence modelling in the design of a novel delivery system for a single-belt steel casting process

Pedro Gutemberg Q. Netto[a], Roderick I.L. Guthrie[b,*]

[a]*Universidade Federal Fluminense, Av. dos Trabalhadores, 420-Vila, Volta Redonda, RJ, Brazil 27260-740*
[b]*McGill University, M. H. Wong Building, 3610 University Street, Montreal, QC, Canada H3A 2B2*

Received 8 October 1998; received in revised form 2 April 1999

Abstract

In this work, a comprehensive model including heat transfer, fluid flow and solidification was used to evaluate the performance of a novel delivery system for a single-belt steel casting process. This near-net-shape casting, although still in development, is one of the most promising routes for casting of low-carbon steel in large scale. This paper focuses on the performance of a low-*Re* κ–ϵ model that was employed to simulate the three-dimensional turbulent flows fully-coupled with heat transfer and macroscopic solidification. Simulations were run for the intended conditions of caster operation, and the results obtained with the κ–ϵ were compared with the results obtained with an ad hoc viscosity model, where the molecular viscosity was boosted 100 times, uniformly throughout the computational domain. A semi-analytical solution was employed for validating the models and the results showed that the ad hoc viscosity model overestimated the thickness of the solidified shell and underestimated the size of the mushy zone. In addition, in a region close to a corner on the top surface of the reservoir, the ad hoc viscosity model predicted much lower temperatures and premature formation of a solid shell. These findings were confirmed when a ceramic filter was included in the computational domain, to modify the flow towards the cooling belt.

1. Introduction

Despite major developments concerning the quality of steels in the past twenty years, increases in the productivity and efficiency of the various processing steps has been relatively incremental. From the beginning of the 1980s, much research has been directed into the development of so-called 'near net shape casting' processes for commercial scale operations. Near-net-shape casting processes have been developed in the past decade, as an alternative to conventional continuous casting processes. Among their numerous advantages are: energy and capital cost savings, higher productivity and better material properties. Various processes, like roll processes and belt processes are being tested in many different countries [1,2]. Nevertheless, the development of such processes requires massive investments in research. Mathematical modelling can considerably reduce the expenditures needed in the development of these processes, when used at the design stage and in the analysis of initial results.

Regarding the quality of a steel strip produced by a near net shape casting process, this is strongly linked to the feeding system. In a single-belt-caster, the delivery system has major importance. It determines how

* Corresponding author. Tel.: +1-514-398-4755; fax: +1-514-398-4168.
E-mail address: rod@minmet.lan.mcgill.ca (R.I.L. Guthrie)

0017-9310/00/$ - see front matter
PII: S0017-9310(99)00121-0

Nomenclature

a_i	coefficients for the discretization equations
b_w	back wall height
C	morphology constant
C_p	specific heat
C_μ	empirical constant for low-*Re* turbulent models
D	pore size of the porous medium
Da	Darcy number
d_p	thickness of the porous medium
f_L	liquid fraction
f_μ, $f_{\mu l}$	empirical constants for low-*Re* turbulent models
g	acceleration of gravity
h_{tf}	heat transfer coefficient
h_m	metal head
H	enthalpy
H_L, H_S	enthalpy at T_l, T_l, T_s
k	thermal conductivity
k_l	thermal conductivity of the liquid
k_p	thermal conductivity of the filter
k_s	thermal conductivity of the solid
K	empirical coefficient (Eq. (15))
l	reservoir length
L_d	computational domain length
L_f	latent heat of fusion
nz	front wall thickness
Nu	local Nusselt number
P	pressure
q	numerical parameter
R_T	turbulent Reynolds number
S_ϕ	source term associated to variable ϕ
T	temperature
T_{amb}	ambient temperature
T_l	liquidus temperature
T_{melt}	temperature of the liquid metal
T_{ref}	reference temperature
T_s	solidus temperature
u, v, w	velocities in directions x, y, z
u_i	velocity in direction i
u_{is}	velocity of the solid in direction i
u_{ip}	i-velocity in the filter region
v_b	velocity of the belt
$\lvert vel_p \rvert$	resultant velocity in the filter
v_{it}	inlet velocity
W	width of the strip
x_i	i-coordinate in the Cartesian system
X	thickness of the solid shell.

Greek symbols

Γ_{eff}	effective diffusion coefficient
ϵ	rate of dissipation of turbulent kinetic energy
ϵ_{it}	initial rate of dissipation of turbulent kinetic energy
ϵ_l	emissivity of liquid steel
ϵ_p	porosity of the porous medium
κ	turbulent kinetic energy
κ_{it}	initial turbulent kinetic energy
κ_p	permeability of the porous medium
μ	viscosity
μ_{eff}	effective viscosity
$\mu_{eff,p}$	effective viscosity of the filter
μ_t	turbulent viscosity
ρ	density
υ	Forchheimer's inertia coefficient
ϕ	general dependent variable.

Subscripts

eff	effective
L	liquid
p	porous medium
s	solid.

the liquid metal will be fed onto the cooling belt and so is responsible for an even distribution of the metal across the width of the belt and through its thickness [3]. Trying to predict the flow behaviour of the steel and heat transfer rates to the water cooled belt are of undoubted relevance to the final quality of the strip.

A mathematical model was developed with the main purpose of exploring some of the difficulties related to the quality of strips produced by potential single-belt-strip casting processes. For a proposed metal delivery system, a comprehensive mathematical model, including heat transfer, fluid flow and solidification was used as a tool to perform this task. This model includes three-dimensional flow with fully coupled momentum and heat transfer. Turbulence effects as deduced from the standard κ–ϵ equations, as well as flow through porous media, are modelled, since the main feature of such delivery systems is the inclusion of flow modifiers, such as a ceramic filter. The present paper focuses, though, on the beneficial effects of a proper definition for turbulent flow modelling. Since metal flow in the proposed delivery system involves a sharp contraction in the flow adjacent to the exit of the nozzle at the front wall (Fig. 1), the turbulent profile is expected to change dramatically in this region. This requires a

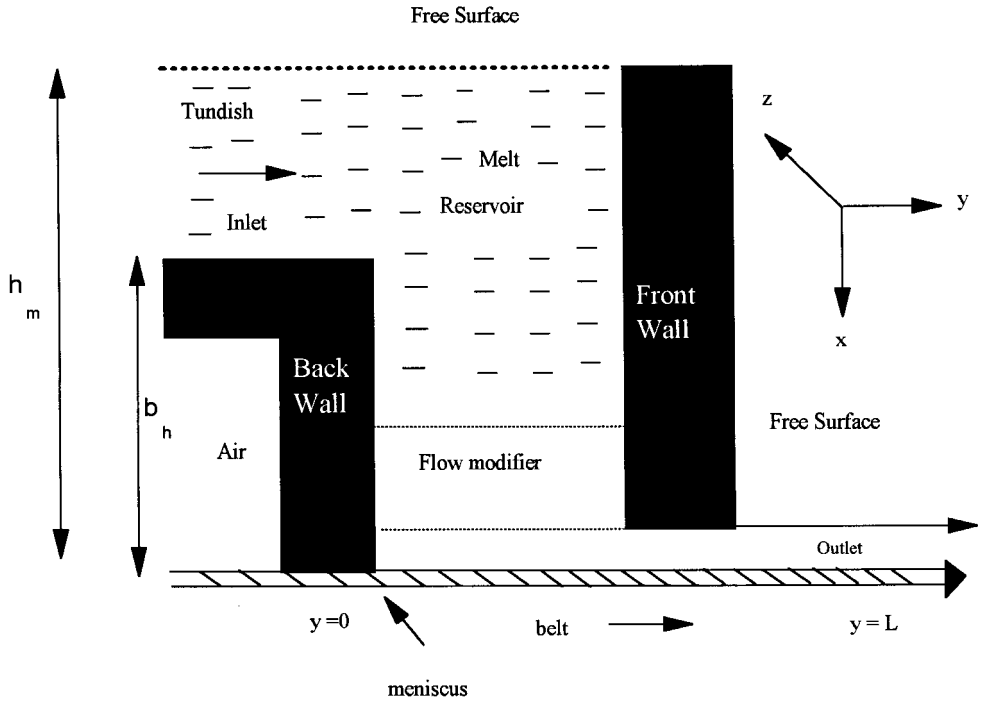

Fig. 1. Schematic of the proposed configuration for the delivery system.

more sophisticated treatment of turbulence effects within the computational domain, than the popular use of an ad hoc constant viscosity model.

2. Development of mathematical model

2.1. General assumptions

The mathematical model respected some predetermined design criteria with respect to geometrical aspects and caster productivity. Other conditions were also superimposed, such as the elimination of any hydraulic jump in liquid exiting the nozzle. To achieve this condition, the specific kinetic energy of the flow in the exit gap ($v^2/2$) was matched to the specific potential energy of the liquid within the extended reservoir (gh). In modelling the energy losses due to friction in the reservoir, these were accounted for using a coefficient of discharge.

Fig. 1 provides a schematic of the computational domain along the longitudinal axis of symmetry. The following general procedure was adopted to determine the primary input data of the model:

1. For a given belt velocity and coefficient of discharge, the metal head was fixed, and the mass flow

Table 1
Values of dependent variable, diffusion coefficient and source terms for the conservation equations

Conservation equation	Variable	Diffusion coefficient	Source term S_ϕ
Continuity	1	0	0
Momentum x-direction U velocity	U	μ_{eff}	$\frac{\partial}{\partial x_i}(\Gamma_\phi \frac{\partial u_i}{\partial x}) - \frac{C(1-f_L^2)}{f_L} + q^3(u-u_s) - \frac{\partial P}{\partial x}$
Momentum y-direction V velocity	V	μ_{eff}	$\frac{\partial}{\partial x_i}(\Gamma_\phi \frac{\partial u_i}{\partial y}) - \frac{C(1-f_L^2)}{f_L} + q^3(v-v_s) - \frac{\partial P}{\partial y}$
Momentum z-direction W velocity	W	μ_{eff}	$\frac{\partial}{\partial x_i}(\Gamma_\phi \frac{\partial u_i}{\partial z}) - \frac{C(1-f_L^2)}{f_L} + q^3(w-w_s) - \frac{\partial P}{\partial z}$
Energy	h	Γ_{eff}	$\frac{\partial}{\partial x_i}[\Gamma_\phi \frac{\partial}{\partial x_i}(H_S - H)] - \frac{\partial}{\partial x_i}[\rho f_s(H_L - H_S)(u_i - u_{is})]$

rate was calculated. Therefore, for the same belt speed, different exit gaps yielded different productivities. In addition, for the same exit gaps, the belt speed was varied, again causing changes in productivity. The metal height was kept as a standard parameter.
2. For those cases where the metal height was varied, the belt speed was kept constant, resulting in a different inlet velocity.

The conservation of mass, momentum and energy can be represented by partial differential equations, whose general form (Patankar [4]) for steady-state flow is:

$$\frac{\partial}{\partial x_i}(\rho u_i \phi) = \frac{\partial}{\partial x_i}\left(\Gamma_{\text{eff}} \frac{\partial \phi}{\partial x_i}\right) + S_\phi \tag{1}$$

where: ϕ = general dependent variable; u_i = velocities u, v and w in directions x, y and z, respectively; x_i = coordinate in the Cartesian system; Γ_{eff} = effective diffusion coefficient for variable ϕ; S_ϕ = source term for dependent variable ϕ.

In Eq. (1), the first term, from left to right, is the convection term, the second term is the diffusion term and the third is the source term. The variable ϕ stands for the different quantities involved in the fluid flow/heat transfer model: velocities u, v and w and enthalpy H. The values of ϕ, Γ_{eff} and S_ϕ are given in Table 1, for the conservation of mass (continuity equation), momentum and energy. The numerical parameter q is introduced to avoid division by zero and the diffusion coefficient for the energy equation has the viscosity and Prandtl number as main physical parameters.

The most important assumptions adopted in the model are listed below:

1. The turbulent fluid flow and heat transfer are fully coupled.
2. The phenomena are essentially three-dimensional and steady-state is assumed.
3. The metal flow is considered incompressible and the fluid Newtonian.
4. Columnar dendritic solidification is assumed.
5. A low-Reynolds number κ–ϵ model was used to account for turbulence within the flow.
6. The Darcy–Brinkman equation was solved for the porous flow control region.
7. Thermophysical properties in the liquid, mushy and solid zones were considered constant.
8. The latent heat is released between the liquidus and solidus temperature in a uniform manner.
9. Natural convection effects are not included in the model, since inertial effects are dominant.
10. The metal is assumed to be laid down on the belt in an isokinetic fashion, i.e., no-slip condition at temperatures equal or below the solidus.
11. Surface tension effects are not considered in the present analysis.

2.2. Solidification

In order to take advantage of the benefits of the fixed grid techniques applied to solidification problems, the continuum model advocated by Bennon and Incropera [5] was used in this work. The main assumptions of this enthalpy–porosity scheme are [5]:

1. The mixture components may be viewed as isolated subsystems, if interactions with other mixture components are properly treated. However, the application of this principle to multiphase, multiconstituent mixtures must take into account that while the phases can be generally considered as isolated, their constituents are often inseparable due to intimate bonding on an atomic level.
2. All properties of the mixture are mathematical consequences of the component properties. However, for non-inert systems, the thermophysical phase properties need to be determined from phase diagrams or empirical equations.
3. The mean collective mixture behaviour is governed by equations similar to those governing the individual components.

As for the flow in the mushy zone adjacent to the thickening strip, it was assumed that the mushy zone behaved as a porous medium. Darcy's law usually applies for columnar dendritic structures and the Carman–Kozeny equation, derived on extension from Darcy's law, was employed. According to Carman–Kozeny's equation, the permeability κ_p is related to the liquid fraction f_L according to:

$$\kappa_p = \frac{f_L^3}{C(1 - f_L^2)} \tag{2}$$

The most significant effect of these permeability source terms will be that of making the v-velocity (direction of movement) of the solidifying shell approach the belt velocity, at the completion of solidification. For the two other directions, the velocity components relative to the freezing strip will approach zero at the points of complete solidification. The source term becomes zero in the liquid zone, and therefore has no influence on the fluid flow and heat transfer.

The constant C (Darcy coefficient) defines the morphology and effectively controls the degree of convection within the mushy zone [6]. Its value should be large enough to force the velocity in the solid region to equal the belt speed in the direction of the movement and to zero in the two other directions. Although it is known [7] that this coefficient needs to be determined

according to the material's microstructure of solidification (dendritic, planar, etc.), values in the range of 1×10^5 to 1.6×10^7 have been reported in the literature. Considering that the cooling rates are very high in the single-belt process, compared to conventional casting processes, a value of 1×10^7 was chosen.

As previously noted, the latent heat is uniformly released between the liquidus and solidus temperatures. This means that the enthalpy behaves linearly over the solidification interval:

$$H = \int_{T_{\text{ref}}}^{T} C_{\text{p}}\,\mathrm{d}T + L_{\text{f}} f_{\text{L}} \tag{3}$$

where L_{f} is the latent heat of fusion, f_{L} is the liquid fraction and T_{ref} is 25°C. The liquid fraction f_{L} is given by:

$$f_{\text{L}} = \frac{H - H_{\text{S}}}{H_{\text{L}} - H_{\text{S}}} \tag{4}$$

In Eqs. (3) and (4), T_{ref} is the reference temperature, G_{p} is the specific heat, L_{f} is the latent heat of fusion, H_{L} and H_{S} are the enthalpy at the liquidus and solidus temperatures, respectively.

2.3. Turbulence

In this work, a low-Reynolds number model was used to account for turbulence near the walls (front, back and sidewalls). This type of model has been developed recently, to fill the vacuum created by the inapplicability of the wall function models to 'low-Reynolds number' flows. Within the low-Reynolds number κ–ϵ models presented in the literature, the model proposed by Launder and Sharma [8] was employed in this work. This model is easy to implement in solidification problems [9], and has often been used for metallurgical applications [9–11]. The turbulent viscosity μ_{t} is given by:

$$\mu_{\text{t}} = C_{\mu} f_{\mu} \rho \frac{\kappa^2}{\epsilon} \tag{5}$$

where κ is the turbulent kinetic energy, ϵ is the rate of dissipation of κ and C_{μ} is a constant. The function f_{μ} is proportional to the turbulent Reynolds number [8]:

$$f_{\mu} = \exp\left|\frac{-3.4}{\left(1 + \frac{R_{\text{T}}}{50}\right)^2}\right| \tag{6}$$

where

$$R_{\text{T}} = \frac{\rho \kappa^2}{\mu \epsilon} \tag{7}$$

In the mushy zone, a mechanism proposed by Shyy [7] was adopted to damp turbulence:

$$f_{\mu} = \sqrt{f_{\text{L}}} f_{\mu'} \tag{8}$$

where f_{L} is the liquid fraction and $f_{\mu'}$ is the original value of f_{μ}.

Other low-Reynolds number models were considered, but the authors did not expect results very different from the chosen one. This in comparison to the popular ad hoc approach. So, the Launder and Sharma model was considered satisfactory for the current purpose.

2.4. Porous medium

One of the most important objectives of this mathematical model is to simulate the modifications that result from the incorporation of a flow modifier in the proposed metal delivery system. In this regard, the first important point is to determine the nature of the flow. Therefore, a prior investigation of the magnitude of these effects was performed.

As suggested by Beckermann et al. [12], the wall (viscous) effects need to be included in cases of a high Darcy number. For this model, the Da number can be calculated by:

$$Da = \frac{\kappa_{\text{p}}}{d_{\text{p}}^2}, \quad \text{where } \kappa_{\text{p}} = \frac{\epsilon_{\text{p}} D^2}{32} \tag{9}$$

In the equation above, d_{p} is the thickness of the filter and D is the filter average pore diameter. Since the permeability of the filters suitable to this kind of application (zirconia or alumina) is in the range of 10^{-8} to 10^{-9} m^2 and the filter thickness is typically 1 or 2 inches, the Da number will range in the neighbourhood of 10^{-5} to 10^{-4}, which is fairly high.

Therefore, the three flow resistances were initially taken into consideration.

1. The bulk damping resistance due to the porous structure (Darcy's law).
2. The resistance due to inertial effects (Forchheimer's extension).
3. The viscous resistance due to the boundary walls (Brinkman's extension).

The general form of the modified momentum equations for porous media is [12]:

$$0 = -\frac{\partial P}{\partial x_i} + \nabla(\mu_{\text{eff, p}} \nabla u_i) - \left(\frac{\mu_{\text{eff, p}}}{\kappa} + \frac{\rho \upsilon \mid vel_{\text{p}} \mid}{\sqrt{\kappa}}\right) \tag{10}$$

$$\mid vel_{\text{p}} \mid = \sqrt{u_{\text{p}}^2 + v_{\text{p}}^2 + w_{\text{p}}^2} \tag{11}$$

$$\kappa_p = \frac{\epsilon_p D^2}{32} \tag{12}$$

where: u_i = velocities u, v and w, in directions x, y and z, respectively, in m/s; x_i = rectangular coordinates x, y and z in m; κ_p = permeability of the porous medium in m^2; ϵ_p = overall porosity of the porous medium; D = average porous media pore size in m; υ = inertia coefficient of Forchheimer's extension = 0.55 [12].

The first results showed, however, that the Forchheimer term did not yield appreciable change in the flow results, only increasing computational complexity. Therefore, for the sake of simplicity and computational savings, this term was not employed for the parametric studies. Indeed, as McDonald et al. [13] had concluded, for *Re* less than 300, the flow is laminar inside the porous medium and thus the inertial terms should not be significant. In the specific problem, *Re*, defined on the basis of pore diameter, ranged typically from 40 to 80.

2.5. Turbulence modelling for flow in porous media

To the best of the authors' knowledge, there is no tested nor experimentally validated model for turbulence generated during flow within a porous medium. Some attempts were reported in the literature, such as the recent model of Masuoka and Takatsu [14], but these initiatives have raised much controversy. Therefore, the basic approach followed in this work was to apply the κ–ϵ equations to the whole domain, including the porous medium. Since the flow was found to be essentially laminar within the porous medium region, the solution of the κ–ϵ equations in this region was basically unnecessary.

2.6. Boundary conditions and thermophysical properties

The initial and boundary conditions represent one of the most important aspects of any kind of modelling. A proper definition of the boundary conditions is mandatory for the model to be useful in practical applications. Usually, the boundary conditions originate from in-plant measurements of the relevant variables, such as temperature and flow velocity. In addition, correlations and data existent in the literature are used with reasonable accuracy.

In the present case, since the model is supposed to simulate a new design of a hypothetical caster, such information is not available. Therefore, the relevant thermal boundary conditions were approximated according to data published in the literature. Nevertheless, the primary objective of the model is to study the influence of the most important process variables and the changes in the fluid flow and heat transfer resulting from the inclusion of a porous medium in the proposed delivery system, and for that purpose, such approximations are not critical.

The most important thermal boundary condition in the present configuration is the overall heat transfer coefficient between the substrate (belt) and the solidifying shell. This coefficient was considered constant for these simulations.

The following standard boundary conditions were adopted for the turbulent fluid flow:

- No-slip on the solid walls, which means that the velocity components in x, y and z and also κ–ϵ are zero. At the moving belt, the velocity in the direction of the movement, v, will be equal to the belt velocity while the two other velocity components plus κ–ϵ will be zero.
- At the free surfaces of the melt (both within the reservoir and the exiting strip), the gradients of all variables with respect to x will be zero and the velocity perpendicular to the free surface will also be zero.
- At the symmetry plane (direction z), the gradient of all variables with respect to z will be zero as well as the corresponding perpendicular velocity.
- At the outlet (40 cm from the back wall), fully-developed flow was considered. This means that the normal gradient of the v velocity and of the turbulence variables will be set to zero along with the other velocities. In addition, the outflow is related to the inlet and the exit gap, to respect continuity for an incompressible liquid.
- At the inlet, the velocity v is specified and linked to the outflow. Velocities u and w are set to zero. The inlet conditions for the turbulence variables were taken from the literature [15], for extended nozzles:

$$\kappa_{it} = 0.005 v_{it}^2; \quad \epsilon_{it} = 0.09 \frac{\kappa_{it}^{1.5}}{0.03(h_m - b_w)} \tag{13}$$

where v_{it} is the inlet velocity and $(h_m - b_w)$ represents the height of the inlet stream.

The energy boundary conditions were, in general:

- The metal loses no heat to the back and lateral walls, i.e., adiabatic conditions were assumed on these walls.
- An initial superheat was specified for the inlet flow.
- The metal on the free surfaces of the reservoir and exiting gap lose heat to the environment by radiation and convection.
- Heat is exchanged by conduction with the side and the bottom of the front wall. A uniform heat flux condition was applied to both sites, equal to 50 kW/m^2.
- The metal primarily loses heat by convective exchange with the substrate (moving belt). Since the main objective of this work is to investigate the

Table 2
Thermophysical properties of the low-carbon steel and porous media

Low-carbon steel	Porous media—92% Al203 foam filters 45 ppi	Porous media—zirconia ZTA 10 ppi
Density, $\rho = 7020$ kg/m^3	Pore size, D = 420 μm	Pore size, D = 1443 μm
Thermal conductivity, k = 32.6 W/m K	Overall porosity, $\epsilon_p = 0.84$	Overall porosity, $\epsilon_p = 0.87$
Specific heat, $C_p = 680$ J/kg K	Thermal conductivity, $k_p = 1.4$ W/m K	Thermal conductivity, $k_p = 2.1$ W/m K
Heat of fusion, $L_f = 270$ kJ/kg		
Solidus temperature, $T_s = 1492$°C		
Liquidus temperature, $T_l = 1535$°C		
Molecular viscosity, $\mu = 0.0068$ kg/m s		
Heat transfer coefficient/air = 10 W/m^2 K		
Emissivity of liquid steel, $\epsilon_l = 0.28$		

different approaches for turbulent flow modelling, and its consequences in the fluid flow and heat transfer predictions, the overall heat transfer coefficient was considered constant and equal to 5000 W/m^2 K.

- On the outlet, a fully-developed profile was considered for the enthalpy.

The thermophysical properties of the low-carbon steel and porous media are presented in Table 2. The values of heat fluxes applied to the walls and the overall heat transfer coefficient are based on industrial data and experimental observation [16].

3. Numerical model

The fully-coupled, nonlinear, partial differential (conservation of mass and energy and momentum equations) cannot be solved analytically. Therefore, a control-volume finite difference scheme based on the SIMPLE algorithm (Semi-Implicit Method for Pressure Linked Equations) was employed. The conservation equations were then discretized into algebraic equations and solved with the in-house METFLO code.

Convergence was achieved when the summation of the individual residuals of the conservation equations was smaller than 0.5%, for each variable. The residuals were calculated based on the inlet quantities. An average number of 3000 iterations were necessary to achieve convergence in a Silicon Graphics Challenge L 100 MHz, each iteration requiring approximately 35 s of CPU time. Grid dependency was investigated for the standard cases, with and without the filter. For the case without the filter, a 72 × 56 × 23 grid was chosen, after calculations showed that finer grids would yield variations in typical results that were not worth the extra computational time, as depicted in Figs. 2 and 3.

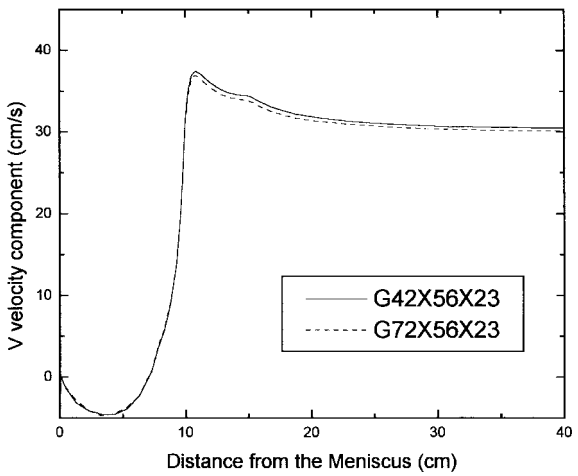

Fig. 2. Grid dependence of the velocity v at 5 mm above the substrate.

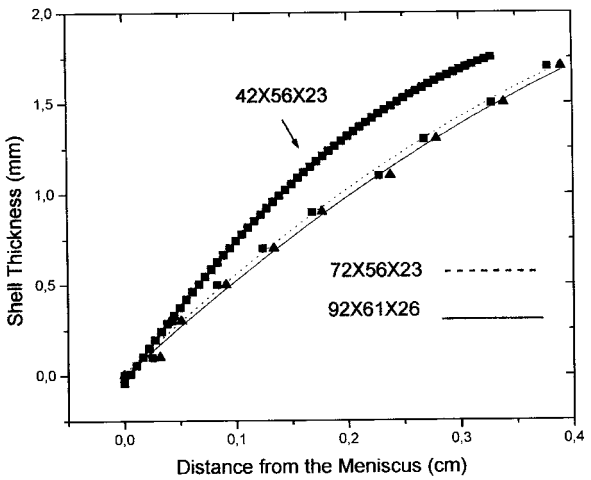

Fig. 3. Grid dependence of the solidified shell thickness.

Table 3
Standard conditions for the simulations of low-carbon steel strip casting

Symbol	Description	Standard value
d_g	Exit gap, strip thickness	10 mm
h_m	Metal head	7 cm; 14 cm (filter)
l	Reservoir length	10 cm
L_d	Computational domain length	40 cm
b_w	Back wall height	4 cm
d_p	Filter thickness	2.5 cm
nz	Front wall thickness	2.25 cm
W	Width of the strip	45 cm
v_b	Belt velocity	1 m/s
S_h	Initial superheat	10°C
m'	Inlet flowrate	114 tph

These figures show only the final step of grid refinement, not all variations in grid density. The values of the velocities and the solidified shell thicknesses were checked in other positions of the computational domain, where fluid flow and heat transfer characteristics were more critical, and the results were confirmed. Table 3 gives the standard conditions for the simulations of low-carbon steel strip casting.

4. Results and discussion

4.1. Importance of turbulence modelling

One of the main purposes of this mathematical model was the inclusion of turbulent flow modelling in

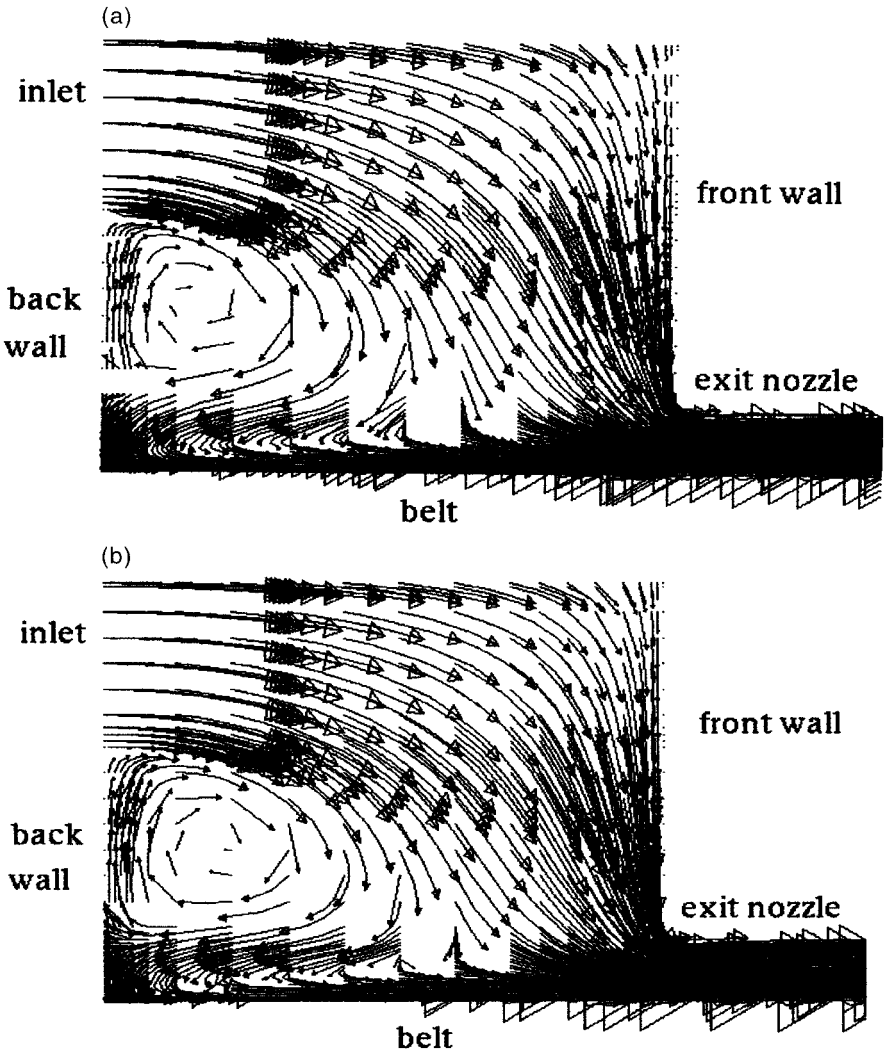

Fig. 4. Vertical cut along the symmetry axis: (a) ad hoc viscosity model; (b) κ–ϵ model.

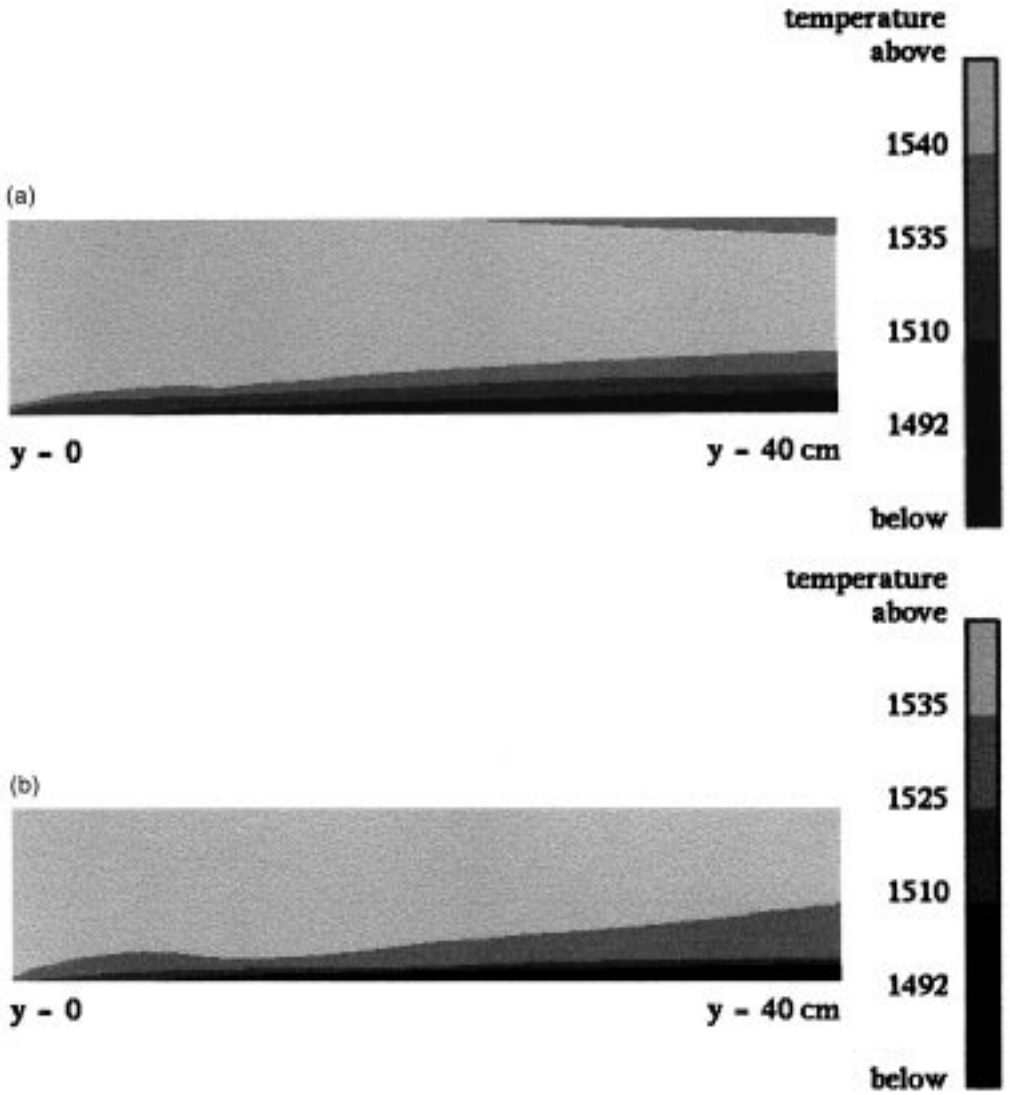

Fig. 5. Temperature profile at the symmetry axis of the strip, for the first 40 cm of the belt: (a) ad hoc viscosity model; (b) κ–ϵ model.

the delivery system. As discussed elsewhere [17], the issue of turbulent fluid flow has inspired various ways to deal with it.

The easiest and most immediate approach is to assign an ad hoc factor to boost the molecular viscosity throughout the domain. This way, the kinematic viscosity will assume a constant value equal to the molecular viscosity times the ad hoc factor in all regions of the liquid metal. Using ad hoc viscosity could work well for cases where the geometry is not very intricate and no large heterogeneities exist within the domain. When the flow follows a smoother path, as for example, in a twin-roll caster, turbulence modelling by κ–ϵ equations may not be very crucial, as may be concluded from Tavares' thesis [11]. In his work, the adoption of an ad hoc viscosity equivalent to the averaged turbulent viscosity (initially calculated by the κ–ϵ model) lead to results qualitatively similar to those obtained with the κ–ϵ model.

There are a few mathematical models for belt-caster processes in the literature. Among them, different approaches were followed for modelling turbulent flow. Farouk et al. [15] used a low-Reynolds number model developed by Spalding and Launder to predict turbulent flow in a twin-belt caster. They followed Asai and Szekely [18], assuming that the molecular viscosity within the mushy zone could be expressed by the same equation used to describe the molecular viscosity in the liquid core, but multiplied by a factor of 20. Truelove et al. [19] presented a fluid flow model for

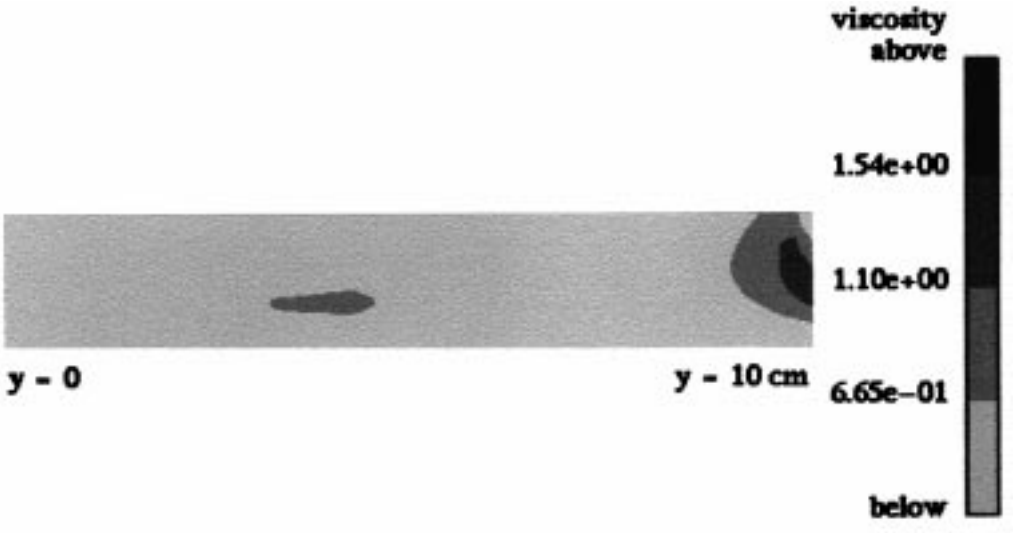

Fig. 6. Turbulent viscosity at the symmetry axis of the strip inside the reservoir.

the single-belt caster that had been in development by BHP Australia. His model included a low-Reynolds κ–ϵ model, but no attempts to include phase-change phenomena were reported.

For horizontal belt casters, Jefferies [20] presented a two-dimensional model, with an artificially boosted viscosity. Despite the usefulness of her results, the use of ad hoc viscosity limits the applicability of her model. As discussed before, the fluid flow in this configuration changes dramatically due to the compression to which it is submitted at the entrance to the exit nozzle. The existence of a recirculation zone and the so-called 'dead zone' near the front wall are also issues of particular relevance. Therefore, the assumption of ad hoc viscosity was replaced with a more realistic one, which in the present case was represented by the Launder and Sharma κ–ϵ model.

To assess the actual implications of the change in strategy to deal with turbulence, simulations were run for the model, taking a constant value of 6.85×10^{-1} kg/m s ($100 \times \mu$) for the viscosity everywhere in the domain. This relatively high value for μ was due to the very turbulent nature of the flow, especially in the region of the nozzle. The results were then tabulated and compared with those given by the Launder and Sharma κ–ϵ model.

4.2. Standard configuration

4.2.1. Fluid flow results

The fluid flow pattern for the case of ad hoc viscosity is shown in Fig. 4(a). The general aspect is the same for the κ–ϵ model (Fig. 4(b)). However, some modifications are noticeable: the recirculation zone is pushed a little backwards and shrinks. The metal on the external recirculation circuit (outside the core) is all dragged down by the cooling belt.

4.2.2. Heat transfer/solidification results

The implications of the ad hoc viscosity scheme on the temperature profiles may be seen in Fig. 5(a) and (b). These figures give the temperature profile in the centre of the strip for the first 40 cm of the belt, for the ad hoc assumption and the κ–ϵ model, respectively. The higher turbulent viscosity (0.685 kg/m s) in the melt–belt interface, as compared to the κ–ϵ model (see Fig. 6), causes premature formation of the solid shell, as predicted by the ad hoc viscosity model. This happens because the heat diffusion coefficient is corrected by the turbulent viscosity value. The formation of the solid shell increases the thermal resistance and therefore, a hotter liquid metal is predicted in the region of the strip inside the reservoir. Almost the entire forming strip is above 1540°C up to the nozzle exit (10 cm from the meniscus). In the nozzle exit region, the ad hoc viscosity in the liquid region is lower than the turbulent viscosity calculated by the κ–ϵ model. This contributes to the banded solidification profile (relatively thin mushy zone and relatively thick solid and liquid phases) exhibited by the ad hoc viscosity model, since it decreases the thermal diffusion coefficient in the liquid zone. At the end of the domain, the dissimilarity is even more evident: on one hand, the solidified shell is thicker (1.3 vs. 1.1 cm); on the other hand, the remainder of the strip is much hotter than in the results given by the κ–ϵ model, as seen in Fig. 5(b). This result is explained by the under-prediction of turbulence by the ad hoc model (for this ad hoc factor), which reduces the heat exchange throughout the

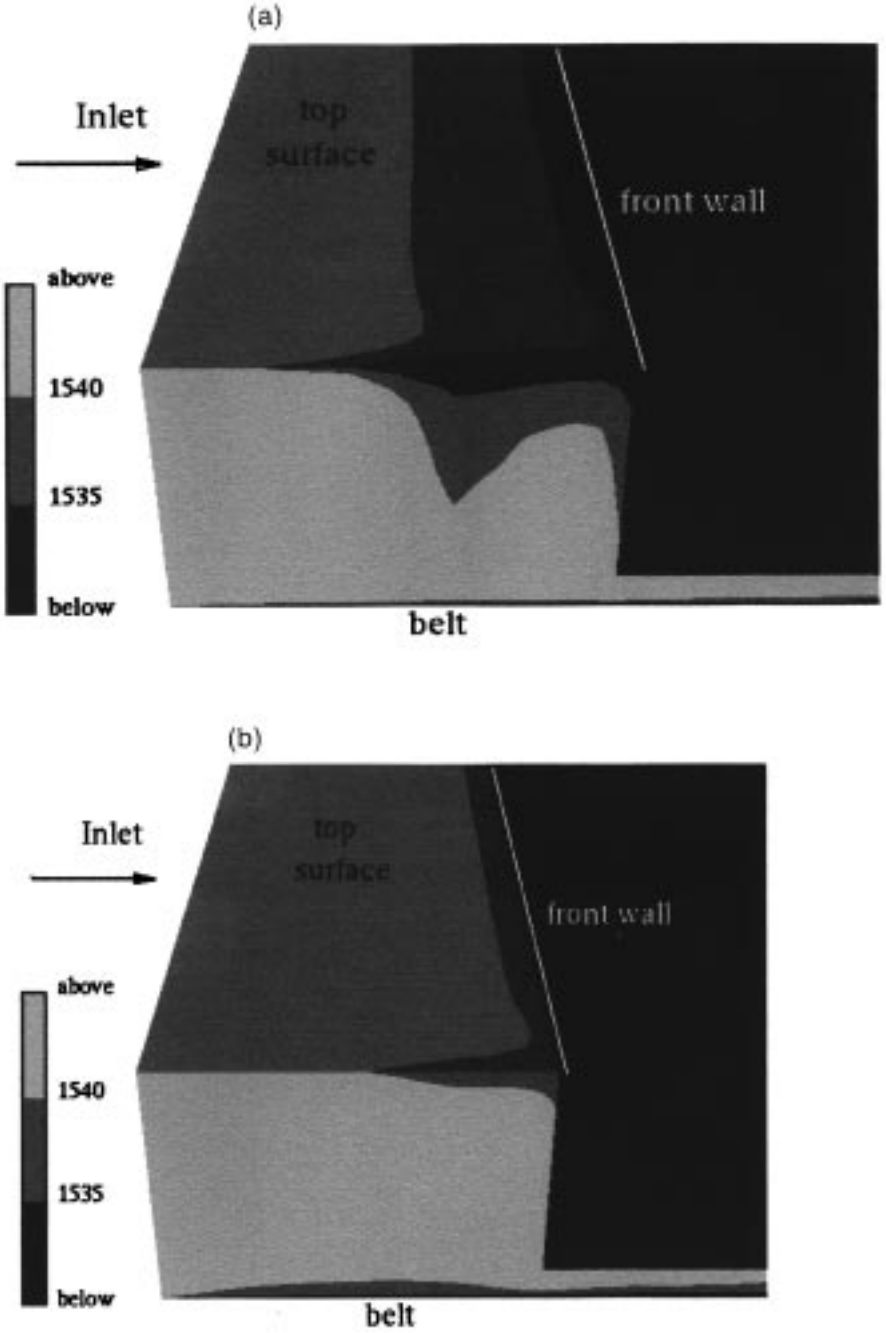

Fig. 7. Temperature profile in the reservoir—detail of the top edge: (a) ad hoc viscosity model; (b) κ–ϵ model.

mushy and liquid regions and contributes to a thicker shell.

Another interesting observation from Fig. 5(b) was than no mushy zone was found on the top surface of the strip at the end of the domain. That would underscore the mechanism of preferential solidification, from the bottom to the top of the strip. Indeed, at the end of the domain only 18% of the strip is mushy, against 40% for the κ–ϵ solution. In the ad hoc solution, the flow is not sufficiently turbulent to transmit the heat losses at the interface shell–belt throughout the thickness of the strip.

4.2.3. Heat transfer/solidification results in the neighbourhood of the front wall

For the region next to the front wall (Fig. 7(a)), the

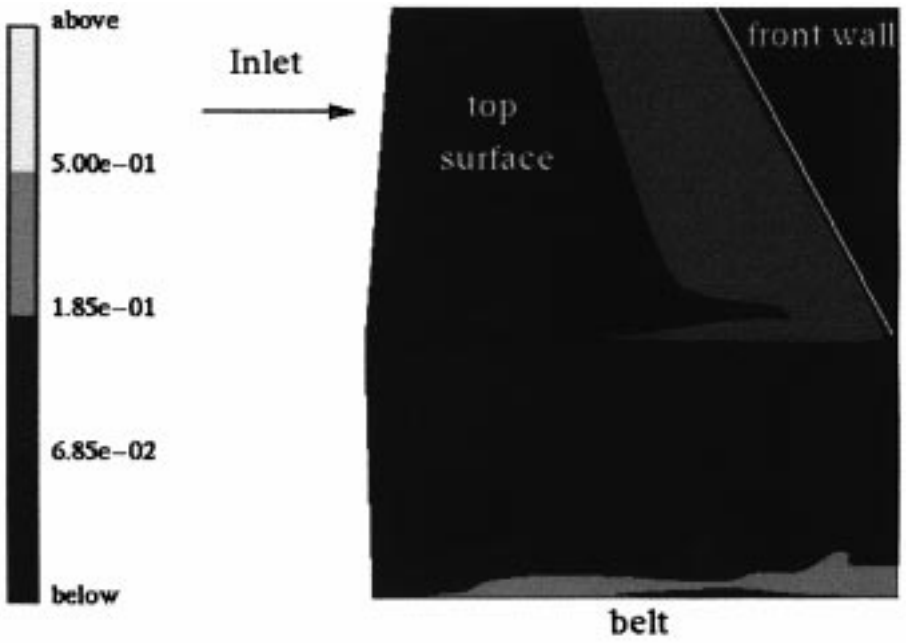

Fig. 8. Turbulent viscosity profile in the reservoir—detail of the top edge.

velocities calculated by the ad hoc viscosity model are lower and therefore, a considerably larger mushy zone appears as a result. In this region, the temperatures are 5°C lower, on average, than the results given by the κ–ϵ model (Fig. 7(b)). This was due to the overestimation of the turbulent viscosity in this region by the ad hoc viscosity model, and consequently, to the overestimation of the turbulent heat diffusion coefficient. Fig. 8 shows the turbulent viscosity profile calculated by the κ–ϵ model. As seen, the values of μ_t in the neighbourhood of the front wall (always less than 0.5 kg/m s) are lower than the value adopted for the ad hoc viscosity (0.685 kg/m s).

From the results presented above, one can readily

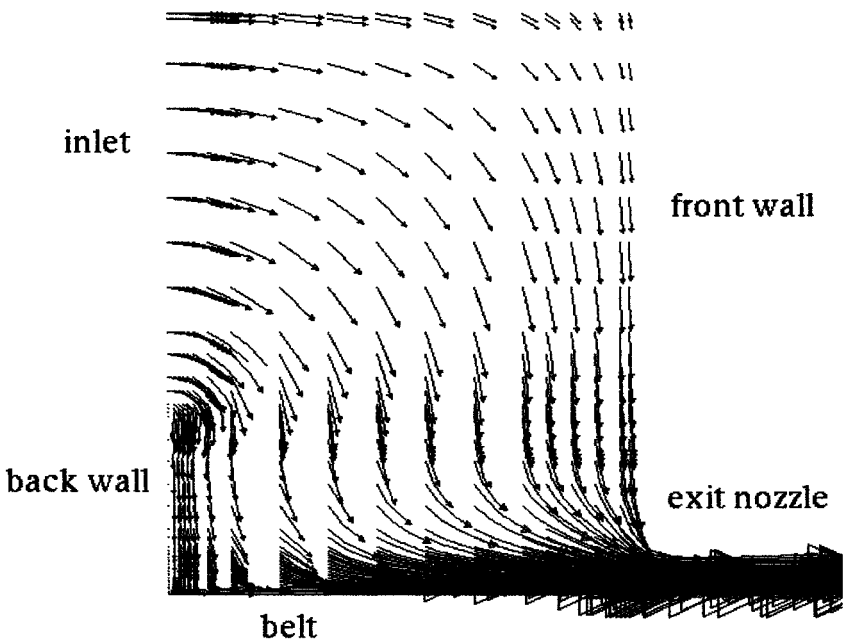

Fig. 9. Vertical cut along the symmetry axis according to the κ–ϵ model—filter included.

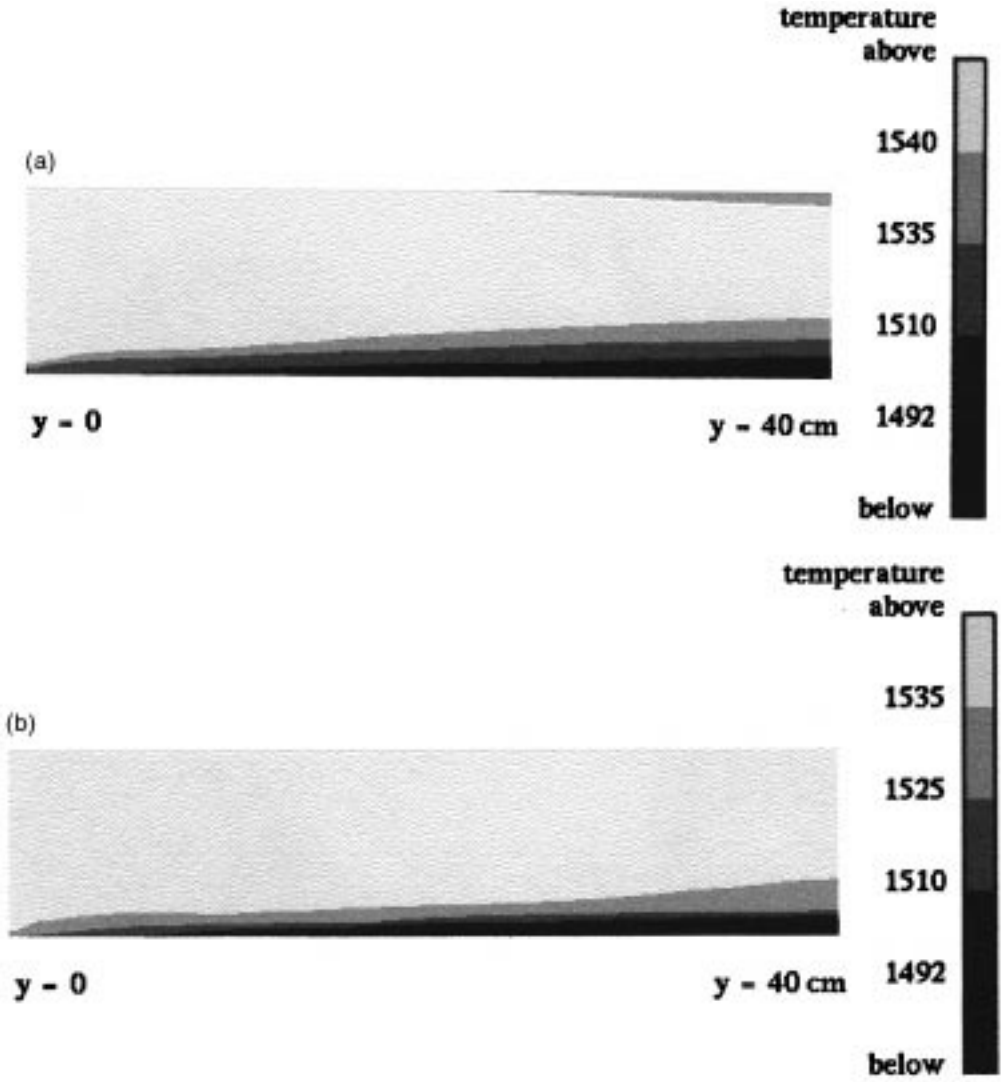

Fig. 10. Temperature profile at the symmetry axis of the strip, for the first 40 cm of the belt—filter included: (a) ad hoc viscosity model; (b) κ–ϵ model.

conclude that the ad hoc viscosity scheme does not work very well for the particular configuration. The existence of a front wall within the computational domain, and the change in flow direction and intensity with the sudden contraction at the nozzle gap constitutes severe limitations to such an approach, because the effect of such heterogeneities in the fluid flow could not be satisfactorily incorporated by the constant viscosity scheme. Accordingly, an over-prediction of the solidified shell thickness and an under-prediction of the mushy zone size is expected using the ad hoc viscosity scheme, for the ad hoc factor of 100.

Using the average value of μ throughout the domain did not change the results much, since, as mentioned before, the turbulent viscosity in the region of the nozzle exit is much higher than the averaged viscosity, whereas in the corner formed by the lateral and front walls the values of μ_t are somewhat lower than the averaged μ. In addition, different values would have to be assigned for the ad hoc viscosity, for every different simulation, in a rather troublesome procedure.

4.3. Filter inclusion

4.3.1. Fluid flow results

Fig. 9 shows the steady-state flow field established within the reservoir zone, for the case where the filter was included in the computational domain, according to the κ–ϵ model. For the case where the ad hoc vis-

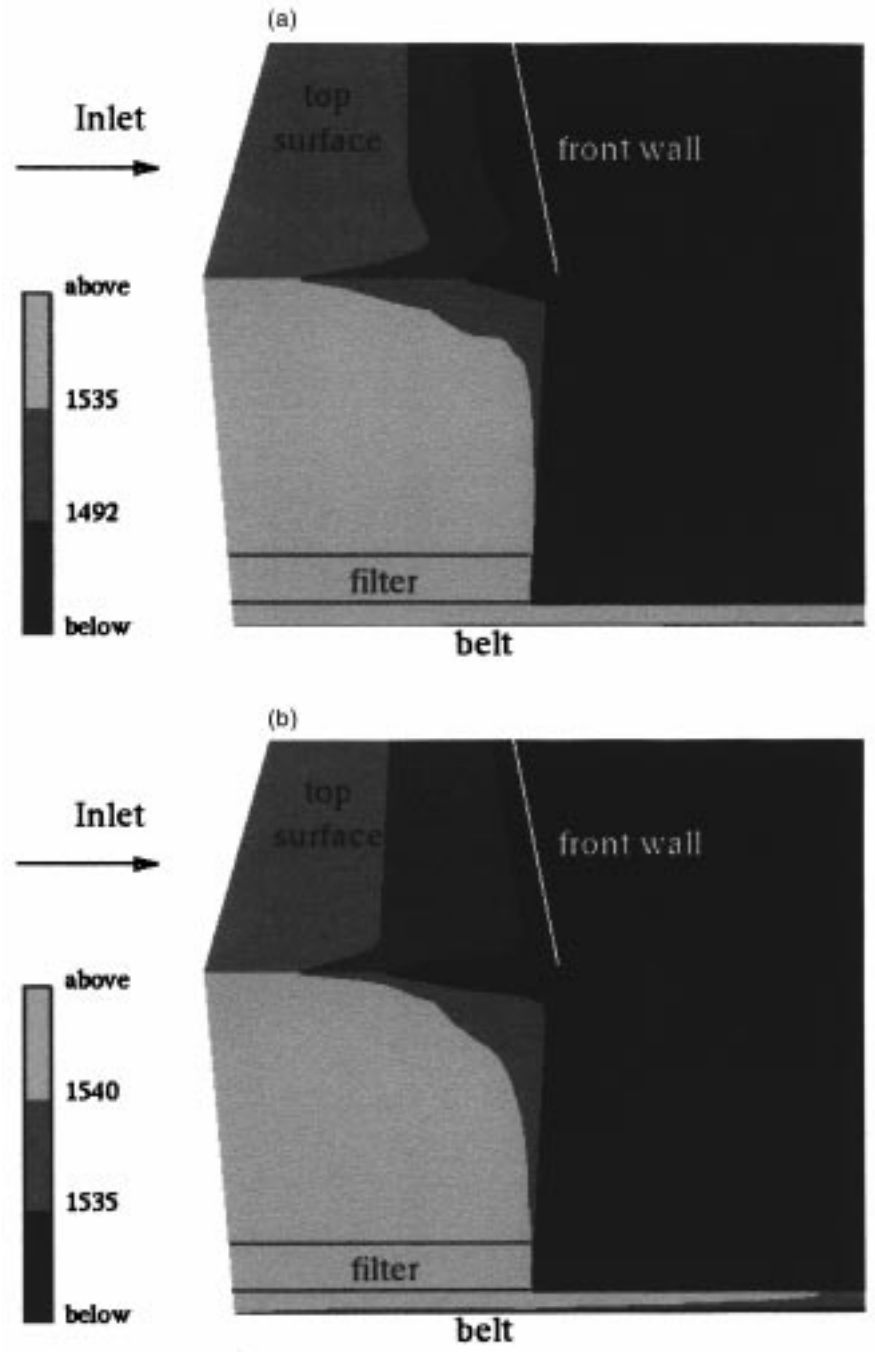

Fig. 11. Temperature profile in the reservoir—detail of the top edge—filter included: (a) ad hoc viscosity model; (b) κ–ϵ model.

cosity was employed, the general characteristics of the flow are similar and little changes were observed.

4.3.2. Heat transfer/solidification results

Fig. 10(a) and (b) depict the temperature profile in the symmetry axis of the strip for the first 40 cm of the belt, for the ad hoc viscosity and κ–ϵ models, respectively. The same trend is observed as in the no-filter case. The ad hoc viscosity model overestimates the thickness of the solidified shell and underestimates the size of the mushy zone.

As for the region near the front wall, again the temperatures are predicted to be much lower than in the κ–ϵ model, as shown in Fig. 11(a) and (b). In Fig.

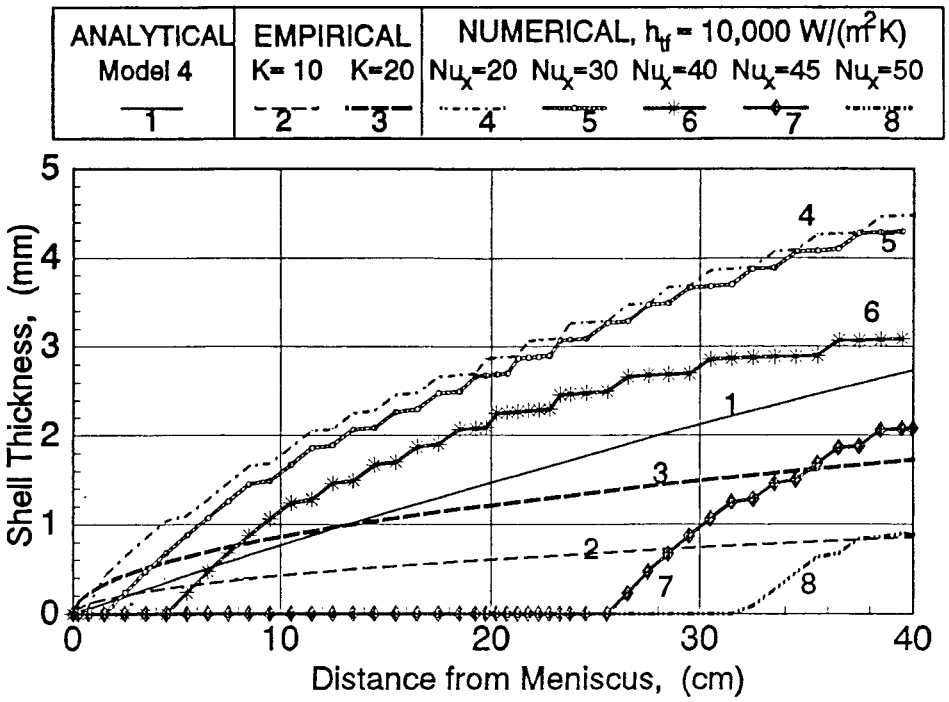

Fig. 12. Predicted shell thickness for some heat flux conditions—Jefferies' work.

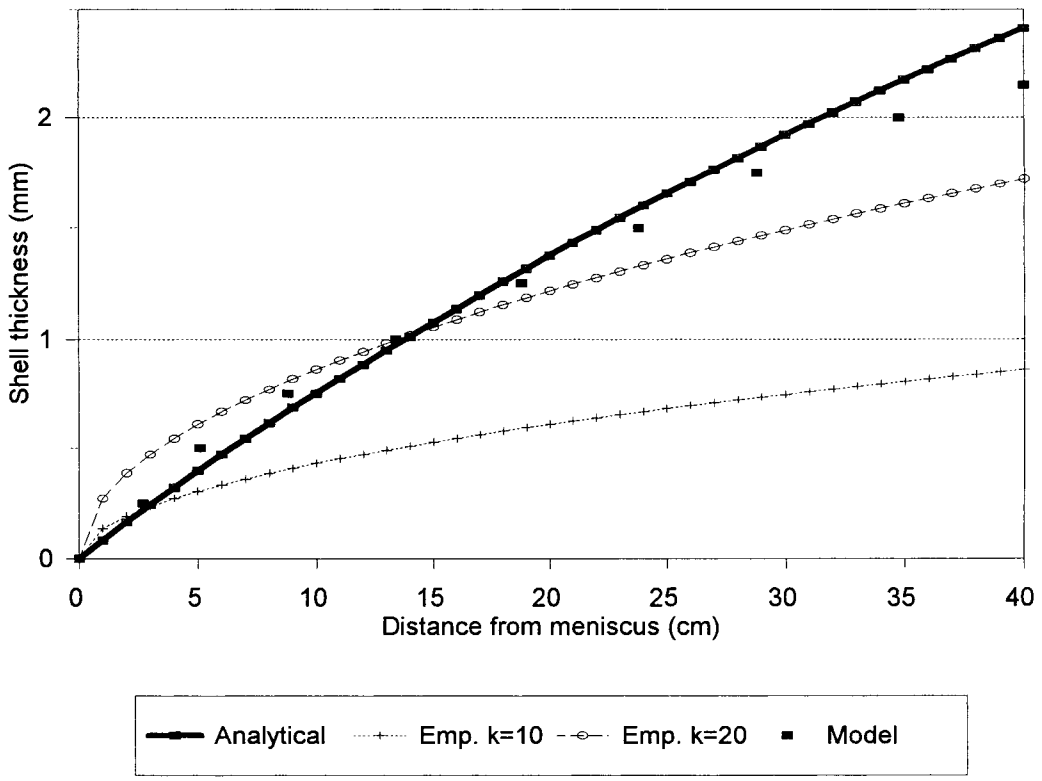

Fig. 13. Predicted shell thickness by the three-dimensional κ–ϵ model.

11(a), representing the predictions of the ad hoc viscosity model, a solid shell even appears in the neighbourhood of the front wall.

5. Comparison with analytical and empirical solutions

In order to validate the model and to compare the results of the ad hoc viscosity model with the κ–ϵ model, the thickness of the solidified shell was calculated for some idealized conditions, using a semi-analytical solution as well as an empirical equation. Adiabatic conditions were considered for all remaining regions of the caster, including the walls and free surfaces, except for the inlet temperature. Fig. 12 shows the predicted thickness for the corresponding thermal boundary conditions, according to Jefferies' model and the semi-analytical and empirical solutions, as detailed in Ref. [20]. To summarize, only the final form of the equations used to calculate the thickness of the solid shell is given below.

5.1. Analytical solution (assuming one-dimensional solidification)

$$X(y) = -\frac{k_s}{h_{tf}} \pm \sqrt{\left(\frac{k_s}{h_{tf}}\right)^2 + \frac{2k_s(T_{melt} - T_{amb})y}{\rho L_f v_b}} \tag{14}$$

where: $X(y)$ = thickness of the solidified shell (m); y = longitudinal position (direction of movement); v_b = belt speed (m/s); k_s = thermal conductivity of the solid shell (W/m K); h_{tf} = overall heat transfer coefficient = 5000 (W/m^2 K); T_{melt}, T_{amb} = initial melt temperature and ambient temperature (K); ρ = density of the metal (kg/m^3); L_f = latent heat of fusion (kJ/kg).

5.2. Empirical solution

$$X(y) = K\sqrt{t}, \quad \text{where } t = \frac{y}{v_b} \tag{15}$$

where K is the solidification constant and it was considered to vary between 10 and 20 mm min$^{-1/2}$.

In Fig. 12, various values of the ad hoc multiplicative factor were tested by Jefferies [20]. In fact, this factor corresponds to the ratio k_{eff}/k_l, which corresponds to the local Nu number at the interface solid–liquid. The two-dimensional ad hoc viscosity model overpredicts the solid shell by as much as 60%, for the lowest values of Nu chosen. For Nu equals to 45, the result approaches the analytical solution at the end of the domain; however, the solidified shell starts at approximately 25 cm from the meniscus and rises much more sharply than the analytical solution. The best results of the two-dimensional model were given by Nu equals to 40, where the solid shell starts at approximately 5 cm from the front meniscus (adjacent to the back wall of the flow system), surpasses the analytical solution at approximately 8 cm and reaches a value approximately 10% higher than the analytical solution at the end of the computational domain. Despite the partial success obtained with the use of an appropriate Nu number, the results of this model are clearly dependent on the right choice of the ad hoc factor and this parameter, being dependent on the local Nusselt number, has to be determined for different relative velocities between the solidifying shell and the molten metal close to it.

As shown in Fig. 13, the predictions of the three-dimensional, κ–ϵ turbulence model are much closer to the analytical solution than those of Jefferies. In Fig. 13, not only is the value at the end of the domain closer, but also the evolution of the solid shell with time is more harmonious for the three-dimensional model. Moreover, considering that the mathematical model solution is not continuous as the semi-analytical one, due to the use of finite grid sizes, the agreement between the three-dimensional κ–ϵ model and the semi-analytical solution (which itself is not exact) is rather good.

6. Conclusions

A comprehensive mathematical model was developed to study fluid flow/heat transfer/solidification phenomena in a novel extended liquid metal delivery system for a single-belt steel caster. The importance of modelling turbulence through the κ–ϵ equations was assessed. The main conclusions drawn were:

- The ad hoc viscosity model over-estimated the thickness of the solidified shell and under-estimated the size of the mushy zone. Solidification occurred first in the region immediately over the belt, due to higher value of the ad hoc viscosity. On the other hand, in the exit nozzle, the ad hoc viscosity was lower than that calculated by the κ–ϵ model dampening turbulence and decreasing the thermal diffusion coefficient in that region. As a consequence, an unusual banded solidification was predicted by the ad hoc viscosity model, with a thicker solidified shell and a thinner mushy zone.
- With respect to the fluid flow in the extended metal reservoir, the profile is virtually the same for both models. However, in the ad hoc viscosity model, the recirculation zone that occurs in the reservoir is pushed a little backwards and shrinks. The metal flow to the recirculating core is drawn down by and towards the cooling belt.
- In the neighbourhood of the front wall, the ad hoc

viscosity model predicted higher values for the turbulent viscosity than the κ–ϵ model. Therefore, the velocities calculated were lower and as a consequence, an enlarged mushy zone was predicted.

- The results for the simulations including the flow modifier confirmed the findings above. Therefore, the κ–ϵ model proved to be a more precise tool in the design stage of the proposed alternative delivery system.
- Semi-analytical solutions together with an empirical equation were employed to validate the model, in terms of the predictions for the solidified shell thickness. It was found that the thickness of the solid shell calculated by the improved κ–ϵ model was in good agreement with the semi-analytical solution. This was not observed for the ad hoc viscosity model.

References

[1] A.W. Cramb, Strip casting of steels: current status and fundamental aspects, in: Proceedings of the International Symposium on Near Net Shape Casting in the Minimills, 34th Annual Conference of Metallurgists, CIM, 1995, pp. 355–372.

[2] H. Murakami, Modelling of turbulent flow, heat transfer and solidification in a twin-roll caster, Ph.D. thesis, Department of Mining and Metallurgy, McGill University, 1993, p. 192.

[3] R. Scholz, R. Jeschar, T. Matschullat, U. Uriau, W. Reichelt, Theoretical modelling of an isokinetical steel feeding system for near-net-shape strip casting, Steel Research 64 (1993) 300–306.

[4] S.V. Patankar, in: Numerical Heat Transfer and Fluid Flow, Hemisphere, New York, 1980, p. 197.

[5] W.D. Bennon, R.P. Incropera, A continuum model for momentum, heat and species transport in binary solid–liquid phase change systems—I. Model formulation, International Journal of Heat and Mass Transfer 30 (1987) 2161–2170.

[6] A.D. Brent, V.R. Voller, K.J. Reid, Enthalpy–porosity technique for modeling convection-diffusion phase change: application to the melting of a pure metal, Numerical Heat Transfer 13 (1988) 297–318.

[7] W. Shyy, Y. Pang, G.B. Hunter, D.Y. Wei, M.H. Chen, Modeling of turbulent transport and solidification during continuous ingot casting, International Journal of Heat and Mass Transfer 35 (1992) 1229–1245.

[8] B.E. Launder, B.I. Sharma, Application of the energy dissipation model of turbulence to the calculation of flow near a spinning disk, Letters in Heat and Mass Transfer 1 (1974) 131–138.

[9] M. Reza Aboutalebi, M. Hasan, R.I.L. Guthrie, Coupled turbulent flow, heat and solute transport in continuous casting processes, Metallurgical and Materials Transactions B 26B (1995) 731–744.

[10] S.H. Seyedein, Three-dimensional modeling of various slab and thin-strip twin-roll casting processes, Ph.D. thesis, McGill University, Department of Mining and Metallurgical Engineering, 1997, p. 287.

[11] R.P. Tavares, Vertical twin-roll caster: metal-mould heat transfer, solidification and product characterization, Ph.D. thesis, McGill University, Department of Mining and Metallurgical Engineering, 1997, p. 397.

[12] C. Beckermann, R. Viskanta, S. Ramadhyani, A numerical study of non-Darcian natural convection in a vertical enclosure filled with a porous medium, Numerical Heat Transfer 10 (1986) 557–570.

[13] I.F. Macdonald, M.S. El-Sayed, K. Mow, F.A.L. Dullien, Flow through porous media—the Ergun equation revisited, Industrial Engineering and Chemical Fundamentals 18 (1979) 199–208.

[14] T. Masuoka, Y. Takatsu, Turbulence model for flow through porous media, International Journal of Heat and Mass Transfer 39 (1996) 2803–2809.

[15] B. Farouk, D. Apelian, Y.G. Kim, A numerical and experimental study of the solidification rate in a twin-belt caster, Metallurgical Transactions B 23B (1992) 477–492.

[16] P.G.Q. Netta, Mathematical and physical modelling of a single-belt casting process, Ph.D. thesis, McGill University, Department of Mining and Metallurgical Engineering, 1998, p. 383.

[17] N.C. Markatos, The mathematical modelling of turbulent flows, Applied Mathematical Modelling 10 (1986) 190–220.

[18] S. Asai, J. Szekely, Ironmaking and Steelmaking 3 (1974) 205–213.

[19] J.S. Truelove, T.A. Gray, P.C. Campbell, J. Herbertson, Fluid dynamics in high-speed strip-casting metal delivery systems, in: Proceedings of the International Conference on New Smelting Reduction and Near Net Shape Casting Technologies for Steel, 1990, pp. 773–783.

[20] C. Jefferies, Modelling a novel, thin strip, continuous steel caster delivery system, Ph.D. thesis, McGill University, Department of Mining and Metallurgical Engineering, 1995, p. 204.